Electronic structure and angle-resolved photoemission spectra of vicinal Cu(111) surfaces via the one-step model

R. Eder and H. Winter

Institut für Festkörperphysik, Forschungszentrum Karlsruhe, 76021 Karlsruhe, Germany

The electronic structure of the Cu(332) and Cu(221) surfaces is obtained by the self-consistent screened Korringa-Kohn-Rostocker method. Angle-resolved photoemission spectroscopy (ARPES) spectra for the Shockley-type surface states at binding energies ≤0.5 eV are calculated within the one-step formalism and found to be in good agreement with experimental data. There is a parabolic band, asymmetrically displaced to the boundary of the surface Brillouin zone. We show that the asymmetry occurs only in the ARPES spectra, whereas the underlying surface band structure is symmetric and explain the asymmetry of the ARPES spectra by analyzing the surface state wave function.

I. INTRODUCTION

Vicinal surfaces are generated by cutting a crystal along a plane which is close to, but not exactly parallel to a plane with low Miller indices. In particular, the vicinal surfaces of the Cu(111) surface to be studied in this paper are defined by their surface normal $\boldsymbol{n} \parallel [i,i,i-1]$, with $i=2,3$. The surface normal thus forms the small miscut angle α with the [111] direction, resulting in a surface that resembles a periodic pattern of skew terraces—which may be viewed as "pieces" of (111) surface—and steps, see Fig. 1. Such surfaces are of interest, because the steps represent a periodic perturbation for the electrons, leading to large supercells. The effect of this supercell formation will be most pronounced for the surface states[1] which are known to exist[2,3] on the (111) surfaces of noble metals. The electrons in these surface states may be viewed as forming a low-density two-dimensional electron gas, an appealing system to study various quantum-mechanical effects. In fact, the possibility of manipulating this two-dimensional electron gas by deliberately placing "corrals" of atoms on a (111) surface has attracted considerable attention.[4] Compared to these perturbations by relatively few adsorbed atoms, which can be studied only by site-selective probes such as tunneling microscopes, the periodic array of steps on the vicinal surfaces offers the advantage that a macroscopic number of electrons is affected by them, whence methods like angle-resolved photoemission spectroscopy (ARPES) can be used to study their effect on the surface states. In fact, quite a number of ARPES studies of vicinal Cu surfaces has been performed over the last years.[5–9] It is the purpose of the present paper to add insights from a theoretical study. We present results from a self consistent electronic structure calculation for the Cu(332) and Cu(221) surfaces and a discussion of the surface states and their spectral properties. In the following Sec. II we give a brief technical overview of the calculation and define the physical quantities to be studied. In Sec. III we present and discuss the results of the calculation and their physical implications, and Sec. IV concludes with a brief summary.

II. METHOD

The calculation of the photocurrent was performed within the framework of the one-step model. Building on previous work by Caroli *et al.*,[10] who started out from the Keldysh formalism,[11] Feibelman and Eastman[12] derived the following expression for the the photocurrent at the position $\boldsymbol{R}$, assumed to be remote from the surface

$$
\begin{aligned}
j(\boldsymbol{R}) \propto{}& \frac{1}{2\pi i} \int d\boldsymbol{r}' \int d\boldsymbol{r} \, \Phi_>(\boldsymbol{r}',\boldsymbol{R},\epsilon)^* \\
& \times O(\boldsymbol{r}') G^+(\boldsymbol{r}',\boldsymbol{r},\epsilon-\omega) O(\boldsymbol{r}) \Phi_>(\boldsymbol{r},\boldsymbol{R},\epsilon) \\
={}& -\Theta(\mu-\epsilon) \frac{1}{\pi} \Im \left[\int d\boldsymbol{r}' \int d\boldsymbol{r} [O(\boldsymbol{r}')\Phi_>(\boldsymbol{r}',\boldsymbol{R},\epsilon)]^* \right. \\
& \left. \times G^r(\boldsymbol{r}',\boldsymbol{r},\epsilon-\omega) O(\boldsymbol{r}) \Phi_>(\boldsymbol{r},\boldsymbol{R},\epsilon) \right].
\end{aligned}
\tag{1}
$$

Here G^r and G^+ denote the so-called retarded and Keldysh Green's functions, respectively, which are related by

$$
G^+(\boldsymbol{r}',\boldsymbol{r},\epsilon) = -2i\Theta(\mu-\epsilon)\Im G^r(\boldsymbol{r}',\boldsymbol{r},\epsilon-\omega),
\tag{2}
$$

with μ the chemical potential of the solid. The retarded Green's function in turn is a solution of the equation

$$
(H-\epsilon)G^r(\boldsymbol{r}',\boldsymbol{r},\epsilon) = -\delta(\boldsymbol{r}'-\boldsymbol{r}),
\tag{3}
$$

where it is understood that the energy ϵ has a small positive imaginary part.

Neglecting local field corrections the operators $O(\boldsymbol{r})$ in Eq. (1) can be written as $O(\boldsymbol{r})=-i\hbar a\hat{\boldsymbol{A}}\cdot\boldsymbol{\nabla}$, where a and $\hat{\boldsymbol{A}}$ are the magnitude and polarization vector of the screened vector potential inside the solid. In principle these should be calcu-
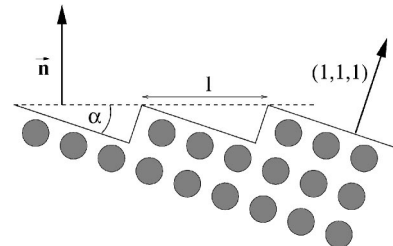

FIG. 1. A vicinal surface.

lated for given direction of the incident light from the Fresnel equations.[13] Since it will be seen, however, that the dependence of the ARPES intensity from the surface state on $\hat{A}$ is very simple, whence no intricate variation with the direction of the incident light is to be expected, and since we are not interested in calculating absolute intensities, we have omitted this calculation.

The so-called low-energy electron diffraction (LEED) state $\Phi_>(r,R,\epsilon)$ in Eq. (1) is defined by

$$\Phi_>(r,R,\epsilon) = e^{-ik\cdot r} + \int dr' e^{-ik\cdot r'} V(r') G^r(r',r,\epsilon). \quad (4)$$

Thereby, $k=\sqrt{\epsilon}$ and the vector k points towards R.

The Green's function G^r can be obtained by means of the Korringa-Kohn-Rostoker (KKR) method.[14] In our version of the KKR formalism, all space is divided into Wigner-Seitz spheres, which are centered on the positions of the nuclei. Within the sphere around the basis atom λ in the unit cell No. j we decompose the position vector r as follows:

$$r = R_j + r_\lambda + \rho,$$

where R_j denotes the position of the unit cell and r_λ the position of the atom within the unit cell (so that $R_j + r_\lambda$ is the position of the nucleus) and ρ the distance from the center of the sphere. Note that for a system with a surface the "unit cell" refers to the group of two-dimensional translations which leave the surface invariant—the unit cell thus in principle has an infinite extension in the direction perpendicular to the surface.

A quantity of interest then is the Fourier transform of the Green's function

$$G_{\lambda',\lambda}(\rho',\rho,\tilde{k},\epsilon) = \frac{1}{N}\sum_{i,j} e^{-i\tilde{k}\cdot(R_i-R_j)}$$

$$G^r(R_i+r_{\lambda'}+\rho',R_j+r_\lambda+\rho,\epsilon), \quad (5)$$

where N denotes the number of two-dimensional unit cells and $\tilde{k}$ is a two-dimensional vector in the surface Brillouin zone—this Fourier transform contains information only about the wave functions with wave vector $\tilde{k}$. Next, we introduce the angular-momentum resolution

$$G_{\lambda',\lambda}(\rho',\rho,\tilde{k},\epsilon) = \sum_{l,m}\sum_{l',m'} g_{\lambda',\lambda}^{(l',m'),(l,m)}(\rho',\rho,\tilde{k},\epsilon)$$

$$Y_{l',m'}(\hat{\rho}')Y_{l,m}(\hat{\rho}). \quad (6)$$

The partial spectral density in the sphere λ then is defined as

$$\rho_\lambda^{(l,m)}(\tilde{k},\epsilon) = -\frac{1}{\pi}\int_0^{R_{WS}} \Im g_{\lambda,\lambda}^{(l,m),(l,m)}(\rho,\rho,\tilde{k},\epsilon)\rho^2 d\rho, \quad (7)$$

where R_{WS} denotes the radius of the Wigner-Seitz sphere (which in principle may depend on λ). It may be viewed as the probability that an electron occupying the state with wave vector $\tilde{k}$ and energy ϵ can be found in the the cell λ and in the angular-momentum channel (l,m) (more precisely it is the mean probability for all states with wave vector $\tilde{k}$ and energy ϵ). The spectral density will be frequently used to

discuss the character of the state in question. For example, its variation with λ gives direct information about the real-space location of the wave function.

The Green's function G^r was obtained by our self-consistent layer code based on the screened KKR method. This differs from the standard version of the KKR method[14] in that the "free" Green's function is replaced by the Green's function for a "reference medium" with a piecewise constant potential.[15] To be more precise, the potential for the reference medium is taken to be large and positive (6 Ryd in the present case) inside the muffin-tin spheres and zero in between. For the energies ϵ of interest the corresponding Green's function then decays exponentially in real space and can be obtained by diagonalizing suitably chosen finite clusters (consisting in our case of three to five shells around a given atom). The method has been described in detail in Ref. 16. To perform the integrations over the two-dimensional Brioullin zone we used the special point method. For the present application 72 points in the irreducible wedge turned out to be sufficient. We fulfill the boundary conditions numerically using the decimation technique.

In a first step we evaluated the Green function, the charge density, the potential, and the Fermi energy for the bulk system by imposing the appropriate boundary conditions. To treat the systems with surfaces in a second step we assumed that 20–40 layers, depending on the surface orientation, are perturbed (intermediate region). In this region we determine the charges self-consistently, whereas to the deeper layers we attribute the bulk charges. For simplicity the atoms were assumed to be at their bulk positions and the relaxations of bond lengths and angles at the surface[17] were neglected. One may expect that the relatively small relaxations will have only a small influence on the ARPES spectra. We employ Broyden's formalism to reach self-consistency after 50–100 iterations and maintain charge neutrality in each step by integrating the Green's function up to the appropriate energy along a rectangular path in the complex energy plane. It is reassuring that the difference between the self-consistent Fermi energy for the surface and the self-consistent bulk Fermi energy turned out to be negligible in all cases. In a third step we use these self-consistent potentials to calculate the Green's functions entering the photocurrent and LEED state on a dense energy mesh parallel to the real axis with imaginary parts of 0.03 eV in the occupied range and 0.03 eV for the LEED states.

Since the single-particle formalism for the Green's function does not contain any damping mechanism, the LEED state does not decay inside the solid. This is unrealistic because the photoelectrons do have a finite mean-free path, and to simulate this effect we have modified the wave function of the LEED state inside the solid according to

$$\Phi_>(r,R,\epsilon) \rightarrow e^{-|z|/\zeta}\Phi_>(r,R,\epsilon), \quad (8)$$

where z is the distance from the surface and the "decay length" $\zeta=20$ a.u. The calculated ARPES spectra are practically insensitive to the choice of ζ within a range of 0–100 a.u.. The combination of one-step formalism for the photocurrent and a KKR-like scheme to obtain the self-consistent Green's functions has been applied previously
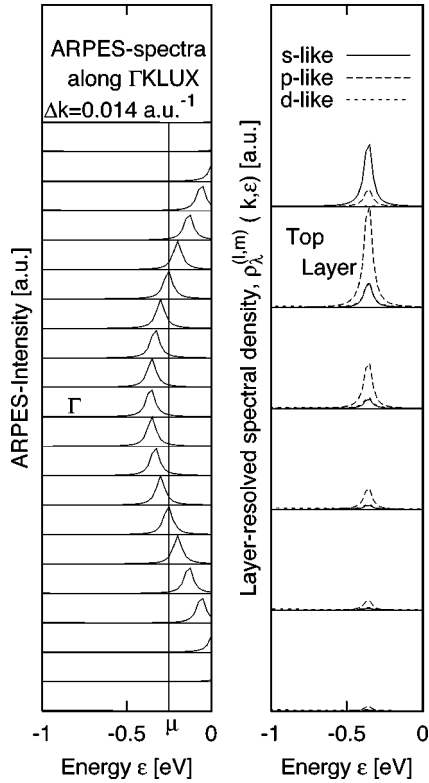
FIG. 2. Left: Calculated ARPES spectrum in the Γ-K-L-U-X plane of the Cu(111) surface. The polarization vector $\hat{A}$ of the incident light is perpendicular to the surface. To give a more continuous dispersion, the Fermi factor $\Theta(\mu - \epsilon)$ has been omitted. The distance in $\widetilde{k}$ space between the individual spectra is δk $=0.014(\text{a.u.})^{-1}$. Right: Layer-resolved spectral density $\rho_\lambda^{(l,m)}(\widetilde{k}, \epsilon)$ at $\widetilde{k}=\Gamma$ (i.e., the bottom of the surface state band).

with considerable success to an analysis of the ARPES spectra of cuprate superconductors.[18–20]

III. RESULTS

We now proceed to a discussion of the ARPES spectra and as a first step we consider in more detail the ideal Cu(111) surface. Figure 2 shows the ARPES spectra in the Γ-K-L-U-X plane of that surface—the parabolic band of the surface state can be clearly recognized. The polarization dependence of the spectrum is very pronounced: only for an electric field perpendicular to the surface (corresponding to grazing incidence and p polarization) is there any appreciable ARPES intensity—in agreement with experiment.[21] The spectra in Fig. 2 refer to that case. Fitting a parabola to the maxima of the intensity yields an effective mass of $m^*=0.434\,m_e$, the bottom of the band is at $\epsilon_B=-0.15$ eV—Baumberger $et\ al.$[8] obtained the values m^* $=0.41(2)m_e$ and $\epsilon_B=-0.391$ eV from their experimental spectra. While the calculated effective mass agrees well with the experimental value, the binding energy at Γ, ϵ_B, is clearly off the mark. Here it should be noted, that the surface state has a low density of states—even a slight inaccuracy in the calculated charge transfer from bulk to surface will therefore
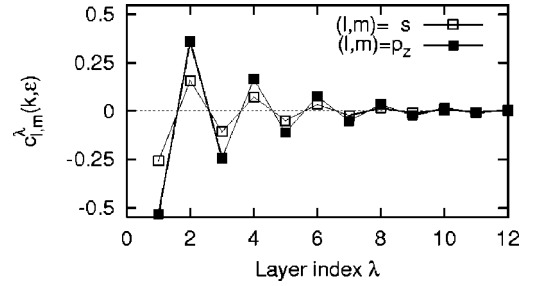

FIG. 3. Wave function expansion coefficients $c_{l,m}^\lambda(\widetilde{k}, \epsilon)$ for the surface state at Γ. The figure shows only the s- and p_z-like amplitudes, which are the dominant ones in the wave function, for graphical reasons the s-like coefficients have been multiplied by (-1).

lead to a rather substantial change of the occupation of the surface band—which will in turn lead to an inaccuracy of ϵ_B. One may expect that the accuracy of ϵ_B can be improved by taking into account the nonspherical part of the potential, i.e., by relaxing the muffin-tin approximation. The muffin-tin approximation clearly is least justified for the atoms near the surface. At present, however, we have not implemented this.

To characterize the nature of the surface state in more detail, Fig. 2 also shows the layer-resolved spectral density, $\rho_\lambda^{(l,m)}(\widetilde{k}, \epsilon)$. Here, λ gives the label of the atomic layer in the z direction. Figure 2 shows that the state in question is a surface state of predominant s-p character. Interestingly the character of the wave function in the first "vacuum layer" changes to a predominant s character. Fitting the peak intensities inside the solid by the exponential law $I(z)=Ae^{-z/L}$, where z denotes the depth of the layer below the surface, yields the decay length $L=4.94$ a.u.—the distance between successive layers is $a_z=a/\sqrt{3}=3.94$ a.u.

Also of interest is the $phase$ of the wave function of the surface state. Omitting the Bloch factor $e^{i\widetilde{k}\cdot R_j}$, the wave function $\Psi_{\widetilde{k},\epsilon}(r)$ can be expanded inside the Wigner-Seitz sphere λ as follows:

$$\Psi_{\widetilde{k},\epsilon}(r) = \frac{1}{\sqrt{N}}\sum_{l,m} c_{l,m}^\lambda(\widetilde{k}, \epsilon)Y_{l,m}(\hat{r})R_l^\lambda(r), \qquad (9)$$

where the radial wave functions $R_l^\lambda(r)$ are normalized according to $\int_0^{R_\lambda} |R_l^\lambda(r)|^2 r^2 dr=1$. The coefficients $c_{l,m}^\lambda(\widetilde{k}, \epsilon)$ can be extracted from the KKR-Green's function. For $\widetilde{k}=\Gamma$, where they are purely real, and the energy ϵ where the spectral density and ARPES spectrum have their maximum, they are shown in Fig. 3. Only the coefficients for s- and p_z-like character have an appreciable amplitude, which immediately explains why for nearly normal emission this state gives appreciable ARPES intensity only for light polarized in the z direction. There is moreover a clear oscillation from layer to layer, i.e., the phase of the wave function of the surface state oscillates with layer number. This is consistent with the notion[21] that the surface state is composed predominantly of bulk states with momenta near the zone boundary momentum $L=(2\pi/a)(\frac{1}{3}, \frac{1}{3}, \frac{1}{3})$ of the bulk Brillouin Zone (BZ) of Cu. The oscillation of the phase of the wave function also

explains the resonant enhancement of the photoemission intensity from the Cu(111)-surface state for specific photon energies.[21] Any wave vector $\boldsymbol{k} \| \boldsymbol{n}$ for which the oscillation of the plane wave $e^{i\boldsymbol{k}\boldsymbol{r}}$ is commensurate with that of the surface state, obviously must obey $\boldsymbol{k} = [(2\nu+1)\pi/a_z]$ with integer ν. Using the expression $E_{\text{kin}} = (\hbar^2 \boldsymbol{k}^2/2m) - V_0$ for the kinetic energy of the final state (with $V_0 = 13.5$ eV),[22] we obtain the photon energies where a resonant enhancement of the ARPES intensity should occur

$$\hbar\omega = \frac{\hbar^2}{2m}\left(\frac{(2\nu+1)\pi}{a_z}\right)^2 - V_0 - \epsilon_F. \qquad (10)$$

With a Fermi energy of $\epsilon_F = -4.5$ eV this gives $\hbar\omega \approx 0$ for $\nu = 0$—consistent with the fact that k_F is very nearly equal to the distance Γ-L. For $\nu = 1$ on the other hand, we obtain $\hbar\omega = 69$ eV, which is very close to the experimental resonance energy reported by Louie *et al.*[21] These authors gave a more sophisticated treatment using an approximate wave function for the surface state, but the physical reason for the resonance is constructive interference between the spatial oscillations of the surface state and the final state wave function. As will be seen later, precisely the same resonance occurs also for the vicinal surfaces, albeit shifted to a higher Brillouin zone.

Finally, we address the width of the peaks in the ARPES spectrum. As already mentioned, the energies in the KKR calculation have to be given a small imaginary part—this is necessary, to ensure the numerical stability of the procedure. Failure to choose a sufficiently large imaginary part results in negative spectral weight and negative ARPES intensity. The width of the peaks in Fig. 2 then are determined by this
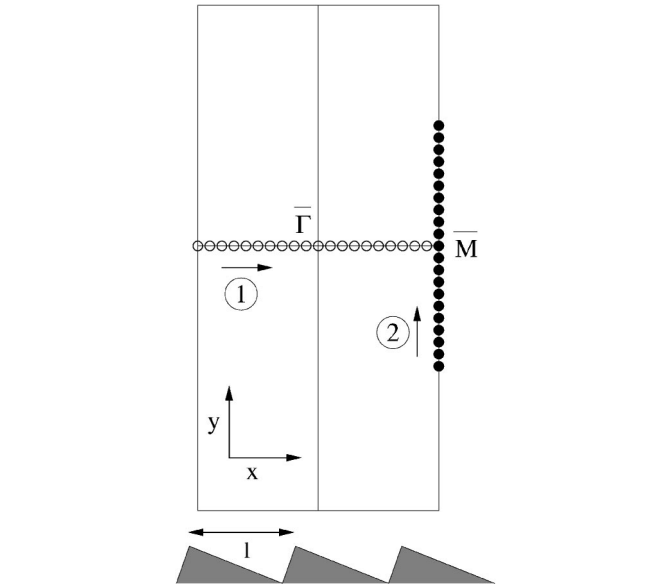

FIG. 4. Schematic plot of the rectangular surface Brillouin zone for the Cu(332) and Cu(221) surfaces showing the two $\tilde{\boldsymbol{k}}$ meshes used for the calculation of ARPES spectra.

"technical broadening" and thus have no real physical significance. Summarizing the data presented so far, we may say that we obtain a clear ARPES signal from a surface state with predominantly s-p_z character, with a decay length of $L \approx 1.2a_z$ into the interior of the solid and with an oscillatory behavior as a function of layer index that is consistent with momenta near the L point of the bulk BZ of Cu.

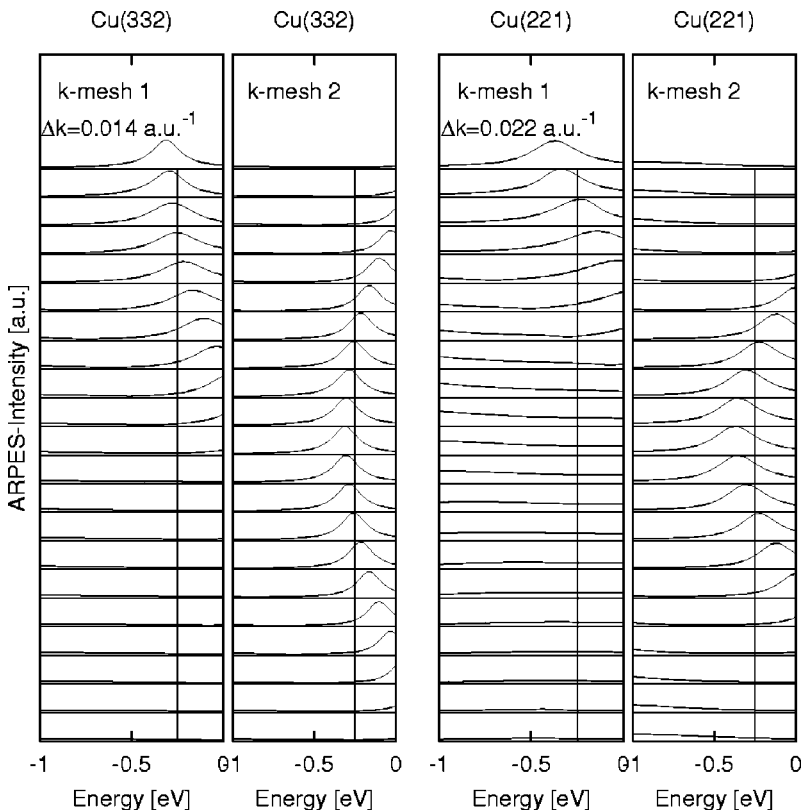After this, we proceed to the vicinal surfaces. Figure 4

FIG. 5. Calculated ARPES spectra for the vicinal surfaces. The figures show the spectra for the $\tilde{\boldsymbol{k}}$ points marked by circles in Fig. 4, the sequence from bottom to top being indicated by the arrows on the respective $\tilde{\boldsymbol{k}}$ meshes in Fig. 4.

TABLE I. Effective masses for the vicinal surfaces in units of the electron mass. The experimental values have been taken from Ref. 8.

	332(calc)	332(exp)	221(calc)	221(exp)
m_x	0.487	0.45(3)	0.317	0.49
m_y	0.467		0.423	
m_y/m_x	0.96	0.87(7)	1.33	1.05(12)

summarizes the geometry of the rectangular surface Brillouin zone as well as the orientation of the coordinate system with respect to the surface steps for the Cu(332) and Cu(221) surfaces. The $\bar{M}$ point is given by $[\pi/l, 0]$, where l is the distance between the surface steps, which can be expressed in terms of the miscut angle α as $l = a_z/\sin(\alpha)$, see Fig. 1. Figure 4 also shows the two $\tilde{k}$ meshes for which ARPES spectra have been calculated. The ARPES spectra themselves are shown in Fig. 5 for both $\tilde{k}$ meshes. Again, there is appreciable intensity only for grazing incidence, and the spectra in Fig. 5 refer to this case. There is overall agreement with the experimental results:[5–8] for the mesh 1 (i.e., perpendicular to the steps) a parabolic band is seen for $k_x > 0$, reaching its minimum at the respective $\bar{M}$. This band also can be seen along the cut through $\bar{M}$ in the y direction. Table I shows the effective masses $m_{\rm eff}$ obtained by a parabolic fit to the energies of maximum ARPES intensity for each $\tilde{k}$ point. The agreement with the experimental values of Baumberger *et al.* for the Cu(332) surface is quite good, whereas the values for the Cu(221) surface differ appreciably. It should be noted, that the peaks are rather broad for (221)—this may explain some of the discrepancy.

As was the case for Cu(111), the binding energy of the band minimum is not reproduced well by our calculation. This implies in particular, that the upward shift of the band bottom with increasing miscut angle[6–8] is not reproduced correctly by our calculation. As already discussed earlier, this probably stems from small inaccuracies in the calculated charge transfer from bulk to surface.

Another feature which is consistent with experiment is the increase of the peak width with increasing tilt angle of the surface away from (111)—see Fig. 5, where the peak width for the Cu(221) surface is discernably larger than that for Cu(332). The full width at half maximum in the calculated spectra is 0.17 eV for Cu(332) and 0.27 eV for Cu(221), the experimental values found by Baumberger *et al.*[8] are 0.28 and 0.48 eV, respectively. The KKR method actually gives directly the Green's function $G(r, r', \epsilon)$ of the electrons, which means that the peak widths in Fig. 5 are really "calculated" and not inserted by hand. As mentioned in Sec. II, for technical reasons the energies ϵ for which $G(r, r', \epsilon)$ is calculated, have to be given a small imaginary part—the corresponding broadening of the peaks, however, is much smaller than the one in Fig. 5. This can be seen from Fig. 2 for the (111) surface, where the peak width is really determined solely by this technical broadening. The much stronger broadening for the stepped surfaces thus reflects a true
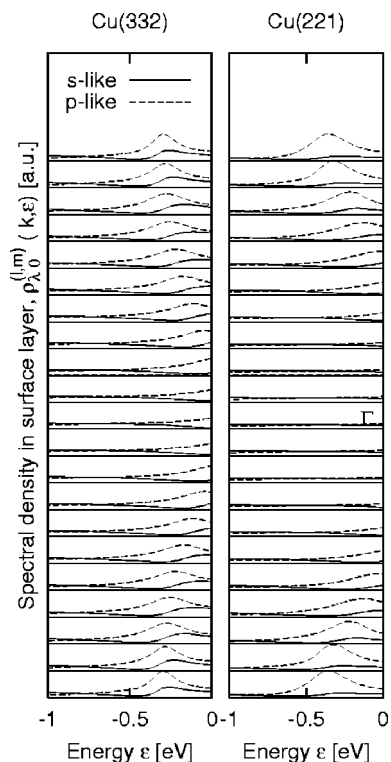

FIG. 6. Partial spectral density $\rho_{\lambda 0}^{(l,m)}(\tilde{k}, \epsilon)$ for the topmost layer of the Cu(332) and Cu(221) surfaces. The momenta $\tilde{k}$ belong to the mesh 1 in Fig. 4 and are arranged in the same order as in Fig. 5.

physical effect. Our "pure single particle formalism" neglects any interaction effects between electrons or between electrons and phonons (or plasmons for the photoelectrons). Since we are dealing with an ideal crystal, variations of the step length or lattice imperfections at the steps are ignored as well. The only possible mechanism within our band-theory formalism is hybridization of the surface state with bulk states. As will be shown later, the data indeed are very consistent with this explanation. An appreciable fraction of the experimentally observed broadening of the surface states thus can be attributed to this hybridization.

We now discuss the ARPES spectra in more detail. The pronounced asymmetry of the ARPES spectra under the exchange $k_x \rightarrow -k_x$ obviously reflects the asymmetry of the stepped surface. In fact, the ARPES spectra seem to suggest that the entire surface state band is simply shifted towards the projection of the L point of the bulk band structure onto the surface normal n.[5] This picture, however, is not really correct: Fig. 6 shows the spectral density $\rho_{\lambda 0}(\tilde{k}, \epsilon)$, with λ_0 the surface layer for momenta $\tilde{k}$ in the mesh 1 of Fig. 4. This might be viewed as the surface band structure weighted by the probability for an electron in the respective state to be in the topmost layer of atoms. Comparison with Fig. 5 shows that this band structure indeed coincides with the ARPES spectrum for $k_x > 0$, but in addition contains a symmetric band portion for $k_x < 0$, which is not seen in the ARPES spectra. For the cut along the x direction, $\rho(\mathbf{k})$ is completely symmetric under the exchange $k_x \rightarrow -k_x$ and thus does not at all reflect the asymmetry intro-
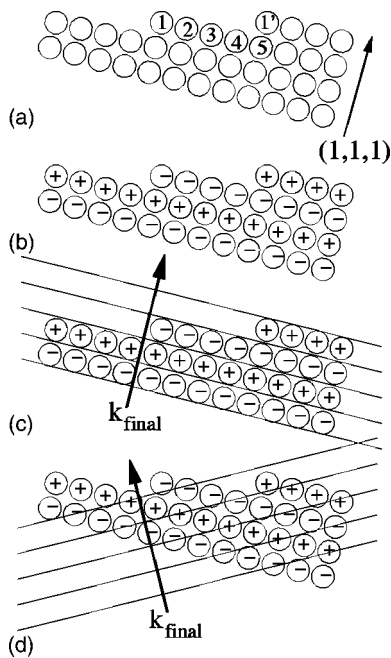
FIG. 7. Mechanism leading to the asymmetry of the ARPES spectrum.

FIG. 8. Expansion coefficients $c_{l,m}^\lambda(\tilde{k}, \epsilon)$ of the surface state wave function at $\tilde{k} = \bar{M}$ for the Cu(332) and Cu(221) surface. The combinations $(l,m) = s$ and $(l,m) = p_z$ are given, which have the largest weight in the wave function. The convention for the assignment of the layer indices λ for the two different surface geometries is indicated in the top part of the figure.

duced by the surface steps (see Fig. 1). In fact, $\rho(\mathbf{k})$ is symmetric under the exchange $k_x \to -k_x$ not due to any spatial symmetry (which does not exist anyway) but due to time-reversal symmetry. In the present case, where there is no magnetic field and spin-orbit coupling is neglected, the spin of the electron does not enter the Schrödinger equation. Since the Hamiltonian constructed by local density approximation is purely real, the complex conjugate of each solution of the Schrödinger equation must be a solution to the same eigenvalue, whence the eigen energies for $\tilde{k}$ and $-\tilde{k}$ must be identical. The asymmetry of the ARPES spectra thus cannot be due to the asymmetry of the underlying band structure—rather it must have its origin in the photoemission process itself.

To understand the mechanism leading to this asymmetry, let us consider the wave function $\Psi_{\tilde{k}, \epsilon}(\mathbf{r})$ near $\tilde{k} = \bar{M}$. To begin with, we note that right at $\bar{M}$ the wave function must be purely real. Next, since we are at the zone boundary, the wave function must change sign when going from one unit cell to the neighboring one in the x direction—whence the wave function has opposite sign at the two atoms 1 and 1′ in Fig. 7(a). On the other hand, one may expect that the phase along the row of atoms $1 \to 5$ in Fig. 7(a) remains constant—this would correspond to a propagation along the corresponding "piece of (111) surface" with momentum $\mathbf{k}_\parallel = (0,0)$. This is the energetically most favorable way to propagate parallel to a (111) surface, so we expect it should be realized at the band minimum $\bar{M}$. Next, assuming that in the direction parallel to [111] the surface state at $\bar{M}$ has the same oscillations in sign as the surface state on the Cu(111) surface (see Fig. 3) we arrive at a picture for the phases of the wave function as schematically shown in Figure 7(b): oscillating in sign along the [111] direction and more or less
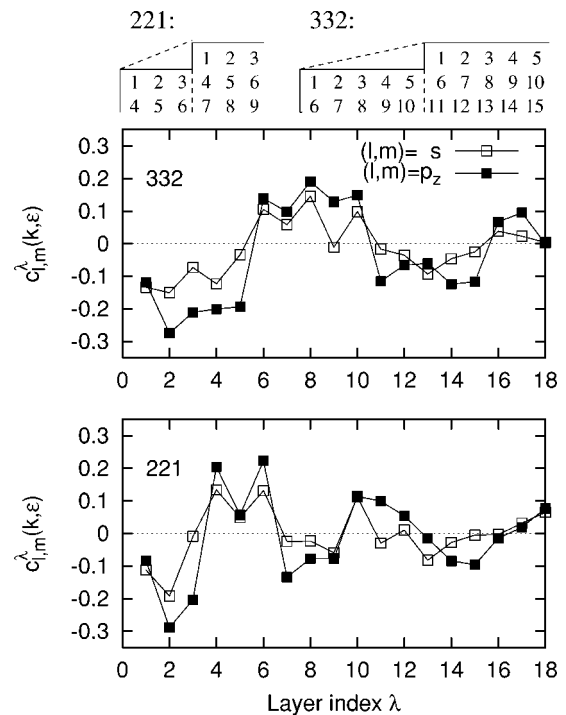
constant within the planes of atoms perpendicular to [111]. This simple picture is in fact corroborated by Fig. 8, which corresponds to Fig. 3 for the Cu(111)-surface state and shows the wave function coefficients $c_{l,m}^\lambda(\tilde{k}, \epsilon)$. The sign of the wave function oscillates if one moves along the [111] direction, whereas it stays constant in the plane of atoms perpendicular to [111]. The wave functions for both, the Cu(332) and Cu(221) surface state at the respective $\bar{M}$ are quite consistent with the schematical picture in Fig. 7(b).

The same picture holds true for the wave functions near $-\bar{M}$ (because $-\bar{M}$ is in fact identical to $\bar{M}$). Then, for ARPES near $\bar{M}$, where the $\mathbf{k}$ vector of the final state is tilted towards the [111] direction, the planes of constant phase of the photoelectron's wave function approximately match those of the wave function of the surface state, see Fig. 7(c). The contributions from the individual atoms within one plane perpendicular to [111] therefore add up more or less constructively and we expect a strong signal in ARPES. For emission near $-\bar{M}$ on the other hand, the wave vector of the photoelectron is tilted away from [111] and the phases do not match—see Fig. 7(d)—whence, we expect destructive interference between the contributions from the different surface atoms and thus no appreciable ARPES signal. This simple picture is in fact confirmed by an analysis of the contributions from the individual atoms to the calculated photocurrent at $\bar{M}$ and $-\bar{M}$. The asymmetry of the ARPES intensity thus is caused

by the different angle between the photoelectron wave vector and the terrace normal at $\bar{M}$ and $-\bar{M}$.

We now want to use this picture for the surface state wave function to determine those photon energies, where the ARPES cross sections at either the $\bar{M}$ point itself or one of the umklapps $\bar{M}+G_\parallel$, with $G_\parallel$ a reciprocal lattice vector of the surface Brillouin zone, is resonantly enhanced. We expect this to happen when the wave vector of the photoelectron is exactly parallel to the [111] direction. We start with the expression

$$\hbar\omega = E_{kin} - \mu = \frac{\hbar^2 k^2}{2m} - V_0 - \mu, \qquad (11)$$

where E_{kin} is the energy of the photoelectron "inside" the solid. In order to have matching between the wave fronts of the plane wave e^{ikr} and the phases of the surface state, we must have $k \parallel (111)$, or $k_\perp / k_\parallel = \cot(\alpha)$. Since we also require $k_\parallel = [(2\nu+1)\pi/l]$ (so as to be at $\bar{M}$ plus a reciprocal lattice vector), the photon energies where the final state wave function matches the phase oscillations of the surface state are given by

$$\hbar\omega = \frac{\hbar^2}{2m}\left(\frac{(2\nu+1)\pi}{l}\right)^2 [1 + \cot^2(\alpha)] - V_0 - \mu. \qquad (12)$$

Since, however, $a_z/l = \sin(\alpha)$, this becomes

$$\hbar\omega = \frac{\hbar^2}{2m}\left[\frac{(2\nu+1)\pi}{a_z}\right]^2 - V_0 - \mu, \qquad (13)$$

i.e., the same condition as for the resonant enhancement of the surface state intensity as for the Cu(111) state, Eq. (10)! Since we have seen there that for $\nu=1$, corresponding to a photon energy of $\hbar\omega = 69$ eV, we had a strong resonant enhancement of the intensity, we expect that the same will occur for any vicinal surface, with the sole difference that the surface state band must be observed around the $\bar{M}$-umklapp $k_x = 3\pi/l$, rather than at $\bar{M}$ itself. The resonantly enhanced image of the surface state thus is shifted to a higher Brillouin zone. It should be noted that for this photon energy we have in fact a kind of "double" resonance: the wave fronts of the photon energies are parallel to the planes of constant phase of the inital state wave function, while at the same time there is the same constructive interference between oscillations in [111] direction as for the Cu(111) surface itself.

To date most studies of surface states on vicinal surfaces have been carried out using photon energies $\leqslant 22$ eV[5–8] and in these studies the surface state has been observed only at $\bar{M} = \pi/l$. Let us therefore estimate the photon energy where the crossover to the point $3\pi/l$ is expected. We expect this to happen when the wave vectors of the two final states with $k_x = \pi/l$ and $k_x = 3\pi/l$ form the same angle with the [111] direction. With the length of the wave vector being given by $k = \sqrt{(2m/\hbar^2)(\hbar\omega - V_0 - \mu)}$ this condition is equivalent to

$$\frac{1}{2}\left(\arcsin\left(\frac{\pi}{kl}\right) + \arcsin\left(\frac{3\pi}{kl}\right)\right) = \alpha, \qquad (14)$$

with α the miscut angle. Numerical solution yields $\hbar\omega = 35$ eV for both vicinal surfaces. Based on the earlier arguments one would expect that for this photon energy the "original" band at π/l and the "umklapp" at $3\pi/l$ have approximately equal intensity, with the umklapp gaining versus the original for higher photon energies. Precisely this behavior has indeed been observed recently by Lobo et al.[9] At a photon energy of 70 eV the parabolic surface state band can be seen only at $k_x = 3\pi/l$, with a considerably enhanced intensity, as compared to 27 eV. At a photon energy of 40 eV both the original band at $k_x = \pi/l$ and the umklapp at $k_x = 3\pi/l$ can be seen, with the original band having somewhat larger intensity. The earlier estimate of 35 eV for the "crossover" thus appears somewhat too simple minded. Apart from that, however, the behavior is exactly as expected on the basis of the earlier considerations, thus confirming our picture of the surface state wave function.

Ortega et al.[6] have inferred a change of the character of the wave function from step-modulated to terrace-modulated from their ARPES data, which is driven by a loss of phase coherence over the terrace length l. One may expect that such a loss of phase coherence should also suppress the resonance at 70 eV, because for phase pattern in Fig. 7(a) a definite phase between the atoms 1 and 1′ is crucial.

Next, we consider the electronic structure in somewhat greater detail, and in particular address the mechanism leading to the broadening of the peaks. Figure 9 shows the layer-resolved spectral density $\rho_\lambda(\tilde{k}, \epsilon)$ for the two vicinal surfaces. For the layers forming the terraces adjacent to the vacuum, one can recognize the predominantly p-like spectral density corresponding to the surface state. The surface state quickly fades away as one moves into the solid, and at a depth of $\geqslant 3a_z$ below the actual surface (measured in [111] direction) additional states of mixed p-d character appear. These states are absent in the spectral density for the ideal Cu(111) surface, see Fig. 2. Their real-space location at several a_z below the actual surface suggests that they are bulk-related, i.e., they are bulk states with wave vectors k along one of the "rods"

$$k(\zeta) = \tilde{k}_\parallel + G_\parallel + \frac{2\pi\zeta}{a}n, \qquad (15)$$

where $G_\parallel$ is one of the reciprocal lattice vectors of the surface Brillouin zone. Were it only for conservation of $\tilde{k}_\parallel$ during the ARPES process, all states with k along these rods could contribute to the ARPES spectra. It should be noted, that the fact that none of these states actually does contribute to the ARPES spectra at $\hbar\omega = 22$ eV is probably not due to the fact that they are "too deep" inside the solid—actually the distance of the respective layers of atoms from the surface is only $\geqslant 2a_z = 8$ a.u., much less than the typical mean-free paths of the photoelectrons. Rather, these bulk states obviously have inappropriate wave vector components perpendicular to the surface.
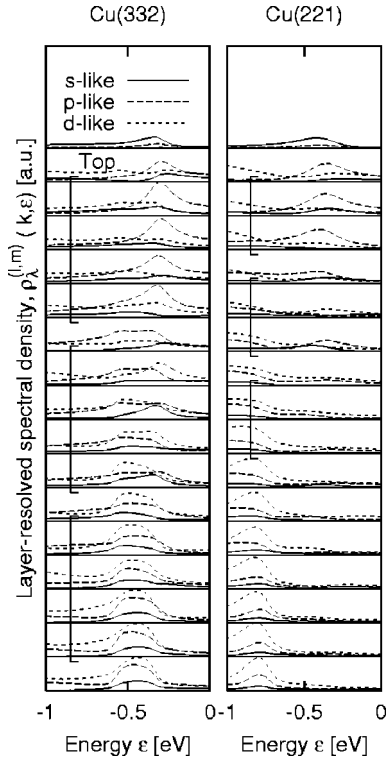
FIG. 9. Layer-resolved spectral density $\rho_\lambda(\tilde{k}, \epsilon)$ at $\tilde{k} = \bar{M}$ for the vicinal surfaces. The sequence of layers is the same as indicated in the top part of Fig. 8. The layers within one bracket therefore are at the same distance (measured along the [111] direction) from the surface.

FIG. 10. (Color online) Layer-resolved spectral density for the edge atom (topmost panel) and the next two atoms along the terrace.

Baumberger *et al.*[8] have suggested, that the hybridization between the surface state and these bulk-related states is the reason for the finite width of the surface state bands, which increases monotonically with the miscut angle.[8] Similarly, Ortega *et al.* have proposed, that mixing between surface state and bulk states near the neck of the bulk Cu Fermi surface is responsible for the crossover from surface-modulated to terrace-modulated wave functions. The layer-resolved spectral density in Fig. 9 is consistent with such a mixing between surface states and bulk states in the following sense: Whereas the surface state on the Cu(111) surface has only a very minor admixture of d character for all layers (see Fig. 2) the surface states on Cu(221) and Cu(332) have—with the exception of the atoms adjacent to the vacuum—a very strong admixture of d character. Since the bulk-derived features also show strong d character, this indicates some mixing between these states.

Even clearer evidence for such bulk-surface mixing, however, comes from the line shape of the spectral density curves in Fig. 6. Figure 10 shows the layer-resolved spectral density for $\bar{M}$ on an enlarged scale, so as to make line shapes better visible. In the topmost layer (corresponding to the atom at the "edge" of the step) the densities for the s, p_z, and $d_{3z^2-r^2}$-like densities show the typical asymmetric Fano line-shape: the combination of a moderate slope at the high energy side of the peak, and a steep slope and a near zero of the curve at the low-energy side. This is particularly clear for the s-like spectral density, less clear for $d_{3z^2-r^2}$ where it is some-
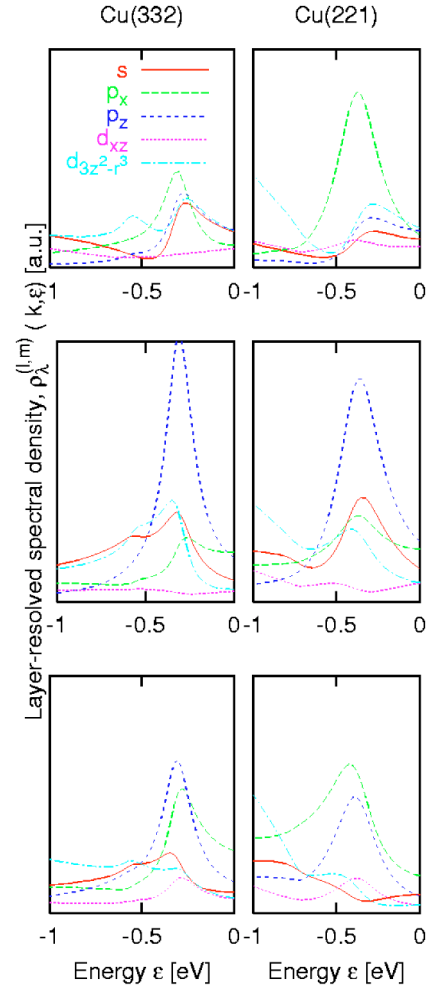
times masked by additional features at lower energies. Such a line shape originates precisely from the mixing between a discrete level (in the present case: the surface state with a fixed $\tilde{k}_\parallel$) and the continuum (here: the bulk states along the "rod" belonging to $\tilde{k}_\parallel$) and thus is clear evidence for a damping mechanism due to surface state—bulk state hybridization. Interestingly the s and $d_{3z^2-r^2}$-like spectral density become increasingly featureless as one moves away from the edge atom—this confirms, that the main mechanism of the broadening is hybridization with bulk states at the step edge atoms.

Figure 10 shows another interesting feature of the surface state: right at the step edge, there is very little p_z-like intensity, but instead a rather strong peak in the p_x-like spectral density. In other words, the p component of the surface state, which usually is nearly parallel to the surface normal, seems to "tilt" at the step edges and orient itself parallel to the surface. For $\tilde{k}$ points along the x direction the wave function must have definite parity under reflection by the (x, z) plane, hence, the p component must be either mixed p_x-p_z or pure p_y. The surface state obviously corresponds to the p_x-p_z mixture, and the angle ϕ_λ which the respective p orbital in the
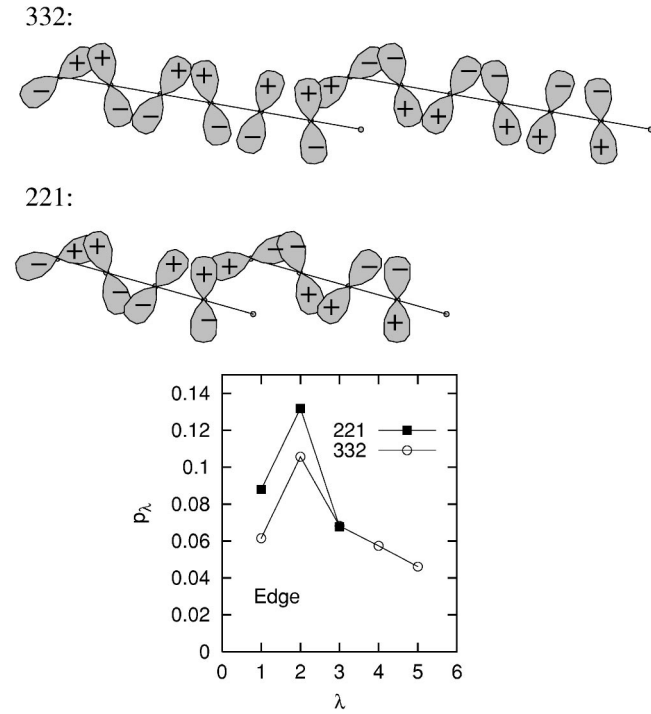
332:

221:

FIG. 11. Top. Direction of the respective p component in the surface state at $\bar{M}$. The tilt angles of the orbitals have been obtained from Eq. (16). Bottom: the amplitude p_λ for the atoms of one terrace.

atom λ is forming with the x axis can be calculated from the expansion coefficients $c_{l,m}^\lambda(\widetilde{\boldsymbol{k}}, \epsilon)$:

$$\phi_\lambda = \arctan\left[\frac{c_{p_z}^\lambda(\widetilde{\boldsymbol{k}}, \epsilon)}{c_{p_x}^\lambda(\widetilde{\boldsymbol{k}}, \epsilon)} \right]. \qquad (16)$$

Figure 11 shows the orientation of the p orbitals for the surface state at $\bar{M}$ obtained in this way. It can be seen nicely that the p orbital right at the step edge tilts so as to bridge the step and connect the two terraces. The p orbitals on the terrace atoms themselves, on the other hand, form a zig-zag pattern. Figure 11 also shows the sum

$$p_\lambda = |c_s^\lambda(\widetilde{\boldsymbol{k}}, \epsilon)|^2 + |c_{p_x}^\lambda(\widetilde{\boldsymbol{k}}, \epsilon)|^2 + |c_{p_z}^\lambda(\widetilde{\boldsymbol{k}}, \epsilon)|^2. \qquad (17)$$

Interestingly, this shows that the amplitude of the wave function is not significantly reduced at the step edge—with the exception of the atom next to the step edge, where it is somewhat enhanced, there is in fact hardly any variation over one terrace. These results have two implications: first, the tilting of the p orbital on the step edges implies that the decay of the wave function as one moves from the surface into the vacuum is stronger at the step edge than on the terraces. This

may explain the results of Sanchez *et al.*,[23] who have reported a depression of the density of states at the edge atoms measured by scanning tunneling microscopy. Second, the result that the amplitude of the surface state is not reduced at the step edge does not support the notion that the step edges act as repulsive potentials for the surface state. Rather, the tilting of the p orbitals away from the ideal [111] direction implies a loss of kinetic energy for the motion perpendicular to the terraces, i.e., in the [111] direction. When going along the [111] direction, the nearest neighbors of a given atom i in the next layer of atoms form an equilateral triangle which has the projection of atom i as its center of gravity. In this situation, the hybridization of the p orbital on atom i with the s and p orbitals on these three atoms is optimal, if the p orbital points in the [111] direction. Exactly this situation is realized for the surface state on the Cu(111) surface at Γ. The tilting of the p orbitals on the vicinal surfaces away from the [111] direction then implies a deviation from this optimal situation, which must lead to a loss of energy from the motion in the [111] direction. This may explain the experimentally observed upward shift of the band minimum at $\bar{M}$ with increasing miscut angle—in fact, the average tilt angle is larger for the Cu(221) than for the Cu(332) surface. There is no indication that the step edges act as a repulsive potential for the surface state.

IV. CONCLUSION

To summarize, we have presented results from a self-consistent surface electronic structure calculation for the Cu(332) and Cu(221) vicinal surfaces of Cu. The calculated ARPES spectra are in good agreement with experiment, the effective masses deduced from the spectra and the calculated peak widths are in reasonable agreement with experimental data. The surface state wave function has predominantly s-p_z character and at $\bar{M}$ it shows a very simple phase pattern, propagating essentially with momentum (0,0) along the terraces and oscillating in sign between atomic layers in the [111] direction. Based on these properties we can readily resolve the apparent discrepancy between an asymmetric ARPES spectrum and a necessarily symmetric band structure, as well as the fact that the resonant enhancement of the ARPES intensity at 70 eV observed for the (111) surface also occurs for the vicinal surfaces, but with the resonantly enhanced image of the surface state being shifted to a higher Brillouin zone. The main mechanism of the broadening of the surface state is mixing with bulk states of predominantly s-$d_{3z^2-r^2}$ character, which takes place at the step edges. The "tilting" of the z orbital in the surface state from being nearly parallel to the surface normal on the terraces to being nearly parallel to the surface may explain the reduction of tunneling current at the step edges, as observed in scanning tunneling microscopy.

[1] W. Shockley, Phys. Rev. **56**, 317 (1939).

[2] P. P. Gartland and B. J. Slagsvold, Phys. Rev. B **12**, 4047 (1975).

[3] For a review see R. Courths and S. Hüfner, Phys. Rep. **112**, 53 (1984).

[4] M. F. Crommie, C. P. Lutz, and D. M. Eigler, Nature (London) **363**, 524 (1993).

[5] A. P. Shapiro, T. Miller, and T.-C. Chiang, Phys. Rev. B **38**, 1779 (1988).

[6] J. E. Ortega, S. Speller, A. R. Bachmann, A. Mascaraque, E. G. Michel, A. Närmann, A. Mugarza, A. Rubio, and F. J. Himpsel, Phys. Rev. Lett. **84**, 6110 (2000).

[7] F. Baumberger, T. Greber, and J. Osterwalder, Phys. Rev. B **62**, 15431 (2000).

[8] F. Baumberger, T. Greber, and J. Osterwalder, Phys. Rev. B **64**, 195411 (2001).

[9] J. Lobo, E. G. Michel, A. R. Bachmann, S. Speller, L. Roca, J. Kuntze, and J. E. Ortega, J. Vac. Sci. Technol. A **21**, 1194 (2003).

[10] C. Caroli, D. Lederer-Rozenblatt, B. Roulet, and D. Saint-James, Phys. Rev. B **8**, 4552 (1973).

[11] L. V. Keldysh Zh. Eksp. Teor. Fiz. **47**, 1515 (1964) [Sov. Phys. JETP **20**, 1018 (1965)].

[12] P. J. Feibelman and D. E. Eastman, Phys. Rev. B **10**, 4932 (1974).

[13] A. Gerlach, R. Matzdorf, and A. Goldmann, Phys. Rev. B **58**, 10969 (1998).

[14] J. Korringa, Physica (Amsterdam) **13**, 392 (1947); W. Kohn and N. Rostoker, Phys. Rev. **94**, 1111 (1954).

[15] A. Lodder and P. J. Braspenning, Phys. Rev. B **49**, 10215 (1994); P. J. Braspenning and A. Lodder, *ibid.* **49**, 10222 (1994).

[16] R. Zeller, P. H. Dederichs, B. Ujfalussy, L. Szunyogh, and P. Weinberger, Phys. Rev. B **52**, 8807 (1995).

[17] R. Heid, K.-P. Bohnen, A. Kara, and T. S. Rahman, Phys. Rev. B **65**, 115405 (2002).

[18] A. Bansil and M. Lindroos, Phys. Rev. Lett. **83**, 5154 (1999).

[19] M. Lindroos, S. Sahrakorpi, and A. Bansil, Phys. Rev. B **65**, 054514 (2002).

[20] M. C. Asensio, J. Avila, L. Roca, A. Tejeda, G. D. Gu, M. Lindroos, R. S. Markiewicz, and A. Bansil, Phys. Rev. B **67**, 014519 (2003).

[21] S. G. Louie, P. Thiry, R. Pinchaux, Y. Petroff, D. Chandesris, and J. Lecante, Phys. Rev. Lett. **44**, 549 (1980).

[22] P. Thiry, D. Chandesris, J. Lecante, C. Guillot, R. Pinchaux, and Y. Petroff, Phys. Rev. Lett. **43**, 82 (1979).

[23] O. Sanchez, J. M. Garcia, P. Segovia, J. Alvarez, A. L. Vazquez de Parga, J. E. Ortega, M. Prietsch, and R. Miranda, Phys. Rev. B **52**, 7894 (1995).